ICES Journal of Marine Science, 2024, Vol. 0, Issue 0, 1–14
https://doi.org/10.1093/icesjms/fsae036
Received: 13 September 2023; **revised:** 12 February 2024; **accepted:** 29 February 2024
Original Article

Quantifying the role of submesoscale Lagrangian transport features in the concentration of phytoplankton in a coastal system

Jacquelyn M. Veatch [1,*], Josh T. Kohut [1], Matthew J. Oliver [2], Hank Statscewich [3], Erick Fredj [4]

[1]Department of Marine and Coastal Sciences, Rutgers, The State University of New Jersey, 71 Dudley Road, New Brunswick, NJ 08901, United States
[2]College of Earth, Ocean and Environment, University of Delaware, 700 Pilottown Road, Lewes, DE 19958, United States
[3]College of Fisheries and Ocean Sciences, University of Alaska Fairbanks, 2150 Koyukuk Dr, Suite 245 O'Neill Bldg., Fairbanks, AK 99775-7220, United States
[4]Computer Science Department, The Jerusalem College of Technology, 21 Havaad Haleumi St., PO Box 16031 Jerusalem 91160, Israel

*Corresponding author. Department of Marine and Coastal Sciences, Rutgers, The State University of New Jersey, 71 Dudley Road, New Brunswick, NJ 08901 United States. E-mail: jveatch@marine.rutgers.edu

Abstract

Food resources in the ocean are often found in low densities, and need to be concentrated for efficient consumption. This is done in part by oceanographic features transporting and locally concentrating plankton, creating a highly patchy resource. Lagrangian approaches applied to ocean dynamics can identify these transport features, linking Lagrangian transport and spatial ecology. However, little is known about how Lagrangian approaches perform in ageostrophic coastal flows. This study evaluates two Lagrangian Coherent Structure metrics against the distribution of phytoplankton; Finite Time Lyapunov Exponents (FTLE) and Relative Particle Density (RPD). FTLE and RPD are applied to High Frequency Radar (HFR) observed surface currents within a biological hotspot, Palmer Deep Canyon Antarctica. FTLE and RPD identify different transport patterns, with RPD mapping single particle trajectories and FTLE tracking relative motion of paired particles. Simultaneous measurements of circulation and phytoplankton were gathered through the integration of vessel and autonomous glider surveys within the HFR footprint. Results show FTLE better defined phytoplankton patches compared to RPD, with the strongest associations occurring in stratified conditions, suggesting that phytoplankton congregate along FTLE ridges in coastal flows. This quantified relationship between circulation and phytoplankton patches emphasizes the role of transport in the maintenance of coastal food webs.

Keywords: lagrangian transport; coastal oceanography; spatial ecology; food web focusing; lagrangian coherent structures

Introduction

Ocean food resources are patchy, concentrated in some areas and sparse in others. This uneven distribution creates ecosystems with fragmented spatial and temporal distribution of both primary producers and their consumers (Benoit-Bird 2023). Food resources (e.g. plankton) must be concentrated either physically or biologically in order to support larger upper trophic species, maintaining a sustainable food supply (Lasker 1978). The processes that govern the attraction of upper trophic species to areas of concentrated food resources is called food web focusing (Genin 2004). As if visiting marine "grocery stores," mobile grazers and foragers rely on concentrated food sources that have been grown elsewhere and transported and concentrated in higher density patches. Besides transport, biological processes can also drive patchiness including population growth, swarming behavior, or predation. Recent studies have demonstrated the importance of physical advection to both concentrate plankton in the creation of these patches (Hofmann and Murphy 2004, Kohut et al. 2018 Oliver et al. 2019) and to maintain connectivity between neighbouring systems sharing resources (Michael et al. 2006). The role of surface currents in the concentration and transportation of plankton has been widely studied in pelagic, open ocean, mostly geostrophic systems on mesoscale and days-long time-scales (Lehahn et al. 2007, Hernández-Carrasco et al. 2011, 2018, Huhn et al. 2012, Li et al. 2015, Lévy et al. 2018, Liu et al. 2018). However, the role of advective transport in more complex, nonlinear, ageostrophic coastal flows is more difficult to characterize. Flow in productive nearshore ecosystems is complicated by tides, buoyancy, highly variable winds, and complex bathymetry, which all contribute to the advection and concentration of plankton patches. This study investigates how coastal ocean currents create localized marine "grocery stores" by transporting and concentrating phytoplankton into discrete patches.

A variety of Lagrangian Coherent Structure (LCS) metrics are used for their ability to quantify advective transport in fluid flows. Attracting LCS are distinct areas within a flow field that have a strong influence on the attraction of neighboring particle trajectories (Farazmand and Haller 2012, 2013, Haller and Beron-Vera 2012, 2013, Haller 2015) using either a single or a paired particle tracking method. When applied to oceanic systems, attracting LCS metrics have the potential to quantify mechanisms of plankton concentration (Huhn et al. 2012), aid in the rescue of overboard passengers (Serra

et al. 2020), and relate ocean features to a variety of biological activity including the migratory patterns of birds (Tew Kai et al. 2009), foraging behavior of apex predators (Cotté et al. 2011, Della Penna et al. 2015, Abrahms et al. 2018) and the distribution and efficiency of fishing vessels (Prants et al. 2014, Watson et al. 2018). This study aims to improve field-wide usage of these metrics by comparing a single particle trajectory metric (Relative Particle Density, RPD) to a more complex paired particle LCS metric (Finite Time Lyapunov Exponent, FTLE). The RPD metric maps regions where particles accumulate, whereas FTLE characterizes how neighbouring particles move relative to each other, diagnosing underlying patterns of trajectories. These two metrics quantify and map unique particle behaviors given the same input ocean circulation. RPD and FTLE were evaluated against alignment with simultaneous observations of phytoplankton patch distribution. Because RPD map accumulation and FTLE identify boundaries between distinct modes of flow, phytoplankton patch centers and edges were distinguished with the hypothesis that RPD will better align with patch centers and FTLE with patch edges. Given these differences in LCS metrics, the following study evaluates the relevance of each to defining phytoplankton patches observed in a complex coastal biological hotspot.

In this manuscript, our approach is to reveal patterns in phytoplankton abundance and advective transport at smaller spatial (O 1 km) and temporal (O 1 h) scales than have been previously examined in ageostrophic coastal flow (Shadden et al. 2009, St-Onge-Drouin et al. 2014). The proper application of LCS metrics allows us to better understand the role of advection in the concentration and transport of plankton patches. The following sections will detail the methodology and results of our comparison between RPD, FTLE, and phytoplankton distribution with a discussion on the implications of using two-dimensional LCS in coastal regions, the differences between single (RPD) and paired (FTLE) particle tracking suggesting when each metric is appropriate, the creation of the interior of phytoplankton patches vs. the border, and how differing levels of stratification affect these relationships.

Materials and methods

Data

The data used in this study are collected from Palmer Deep Canyon, Antarctica in January through March of 2020 as part of a National Science Foundation funded project, SWARM. These data provide coincident dynamic distribution of both plankton patches and underlying physical features over the entire local penguin foraging season. These observations were provided through an integrated polar observatory that included three High Frequency Radars (HFRs), a Slocum glider, and twice-weekly ACROBAT towed surveys between January and March 2020 (Fig. 1). The ACROBAT is small (0.5 m)-winged instrument that profiles the surface ocean (0–50 m), highly resolving light and physical properties. HFRs produce hourly surface current maps at 1 km resolution covering about 1500 km^2, the glider profiled to 1000 m completing one dive (two profiles) every 4 h at the head of Palmer Deep Canyon, and 16 ACROBAT towed surveys (60 km) were completed observing 40 distinct phytoplankton patches (Fig. 1).

Palmer Deep Canyon

Palmer Deep Canyon's relatively short and tightly coupled food web (Saba et al. 2014) makes it a unique ecological laboratory to quantify the impact of concentrating features on phytoplankton. Phytoplankton are a major food sources for Antarctic Krill (*Euphausia superba*), a keystone species for many top predators in the region, including penguins. Penguin colonies surrounding Palmer Deep Canyon have persisted for millennia, according to geologic records (Fraser and Trivelpiece 1996, Emslie et al. 1998, Schofield et al. 2013) despite significant variations in climate conditions. Such endurance of Palmer Deep Canyon's penguin colonies suggests the presence of a strong concentrating mechanism at the base of the food web, able to supply reliable phytoplankton to krill during interannual climate oscillations.

Recent studies in Palmer Deep Canyon have shown the surface residence time scale (∼2 days) is much shorter than the phytoplankton doubling timescale (∼7–70 days) (Kohut et al. 2018). These findings suggest that increased phytoplankton availability in Palmer Deep Canyon compared to neighboring regions is likely due to transport from other regions rather than stimulated local growth from upwelled, nutrient-rich Upper Circumpolar Deep Water as was previously thought (Kavanaugh et al. 2015). Additionally, recent glider observations have been unable to detect nutrient delivery via upwelling during the growing season (Hudson et al. 2019). Even if nutrient availability was higher in Palmer Deep Canyon compared to neighboring regions, phytoplankton in this system have been shown to be light limited rather than nutrient limited (Carvalho et al. 2019). It is within this transport-driven coastal ecosystem that this study investigates the role of Lagrangian features to define the distribution of phytoplankton patches.

HFR

HFRs use doppler-shifted radio waves backscattered off the ocean surface to observe surface velocity. Signals are transmitted and received by an HFR antenna, and Bragg peaks in the measured Doppler spectra are used to calculate radial components of the surface velocity (Barrick et al. 1977). Measured radial components of the surface ocean velocity are directed toward the HFR antenna with a range resolution of 500 m horizontally and 5° in azimuth. Radial components from the three HFR stations are added together to construct magnitude and direction of surface current velocities using an optimal interpolation algorithm (Kohut et al. 2006) providing hourly maps of surface currents at 1 km spatial resolution (Fig. 2a).

The three-site network included two remote locations on the Wauwermans and Joubin islands operated at a center frequency of 25 MHz and a third site at Palmer Station operated at 13 MHz (Fig. 1). The two remote sites located beyond existing power grids used Remote Power Modules constructed on site. More details on the installation of this 3-site network are provided in Statscewich and Weingartner (2011) and Kohut (2014).

The three HFR sites collected hourly radial maps of ocean surface current component vectors over our study area, covering about 1500 km^2 more than 80% of the time (Fig. 2a). The hourly, two-dimensional surface current maps derived from the radial component vector maps provided by each of the three HFR sites were used to derive our two LCS metrics (Fig. 2b and c). Before the LCS calculations were done, gaps within

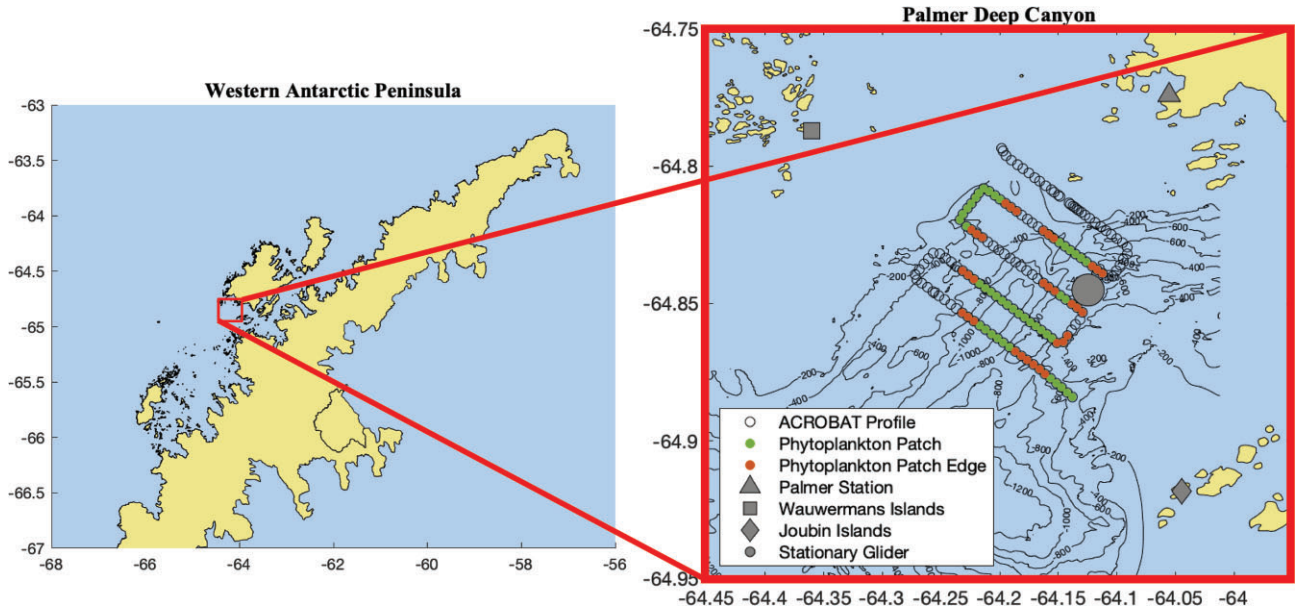

Figure 1 Study area indicating locations of three HFRs (Palmer Station, Wauwermans Islands, and Joubin Islands,) ACROBAT towed survey, and stationary glider around Palmer Deep Canyon, Antarctica. The canyon bathymetry is contoured with 200 m isobars. Plotted is an example of one ACROBAT survey on 12th February 2020, with profiles designation as "phytoplankton patch" and "phytoplankton patch edge." Inset is a map of the Western Antarctic Peninsula, with a box around the study area.

the 80% coverage area of the HFR maps were filled using a rigorous HFR-specific method (Fredj et al. 2016). This follows methodologies in Veatch et al. (2022).

ACROBAT towed surveys

Twice weekly ACROBAT surveys were conducted along transects over Palmer Deep Canyon (Fig. 1) between January and March 2020. The ACROBAT instrument was towed behind a small, (10.2 m) rigid hull boat at ~6 kts (about 3 m s^{-1}) as the instrument undulated continuously between a depth of 1 and 50 m. The ACROBAT was equipped with a fast-sampling (16 Hz) Seabird 43 FastCAT CTD (conductivity, temperature, and pressure), and a Wetlabs Ecopuck optical sensor (chlorophyll-*a* and CDOM fluorescence and optical backscatter at 700 nm). Profiles had a 300-m resolution over the 60-km transect for ~160 vertical profiles per survey. A total of 16 surveys were conducted. ACROBAT data was processed, quality controlled, and profiled using a MATLAB toolbox (Reister 2023) and the methods as described in Martini et al. (2016).

For each profile, the mixed layer depth (MLD) was calculated as the maximum buoyancy frequency in the upper 50 m following methods in Carvalho et al. (2017). For profiles with no clear mixed layer in the upper 50 m, the deepest ACROBAT measurement was designated as the MLD. Phytoplankton abundance was measured as the particle backscatter (m^{-1} sr^{-1}) above the MLD of each profile, integrated using a trapezoidal integration. Particle backscatter was used instead of chlorophyll-*a* fluorescence to negate for effects of nonphotochemical quenching and photo acclimation. Particle backscatter has been shown to correlate linearly with chlorophyll-*a* fluorescence in Palmer Deep Canyon (Carvalho et al. 2016), making particle backscatter a good indicator of chlorophyll biomass. To address the resolution mismatch between the ~300 m separated profiles and the 1-km HFR grid resolution, a sliding filter with a 1-km window was applied to the MLD and particle backscattering data. ACROBAT transects took 4–6 h to complete. It was determined that the ACROBAT did not resample phytoplankton patches that were advected back over the survey from previously sampled waters (Supplementary material S1).

The distribution of phytoplankton patches for each survey were derived from the ACROBAT profiles. To do this, each profile was designated as "phytoplankton patch," "phytoplankton patch edge," or neither. An ACROBAT profile with integrated mixed layer particle backscatter 5% higher than that survey day's median was designated as "phytoplankton patch" following the threshold method from Thomalla et al. (2015). A daily threshold was used for the definition of phytoplankton patches to capture concentrating mechanisms even on days that had lower phytoplankton abundance, which shows a strong seasonal signal. Survey thresholds of particle backscatter ranged from 0.0177 to 0.1184 m^{-1} sr^{-1}. The ACROBAT profiles on either side of the phytoplankton patch, the first and last profile of the phytoplankton patch, and the second and second to last profile of the phytoplankton patch were designated as "phytoplankton patch edges" (Fig. 1), following methodologies in Veatch et al. (2022). Deciphering between patch interior and edge will be used to test for differences in the horizontal advection mechanisms that created the center of accumulation and where the patch ended. Phytoplankton patches that were less than a kilometer and a half long were not used in analysis given that the 1-km resolution of the HFR input data likely did not resolve advective transport that created a phytoplankton patch that small.

Stratification was calculated from the ACROBAT CTD data as the density difference between the surface and 50 m for each ACROBAT profile. "Stratified surveys" were defined as the 8 survey days with the highest average density difference and "mixed surveys" were defined as the surveys with the lowest average density difference (Figure S1).

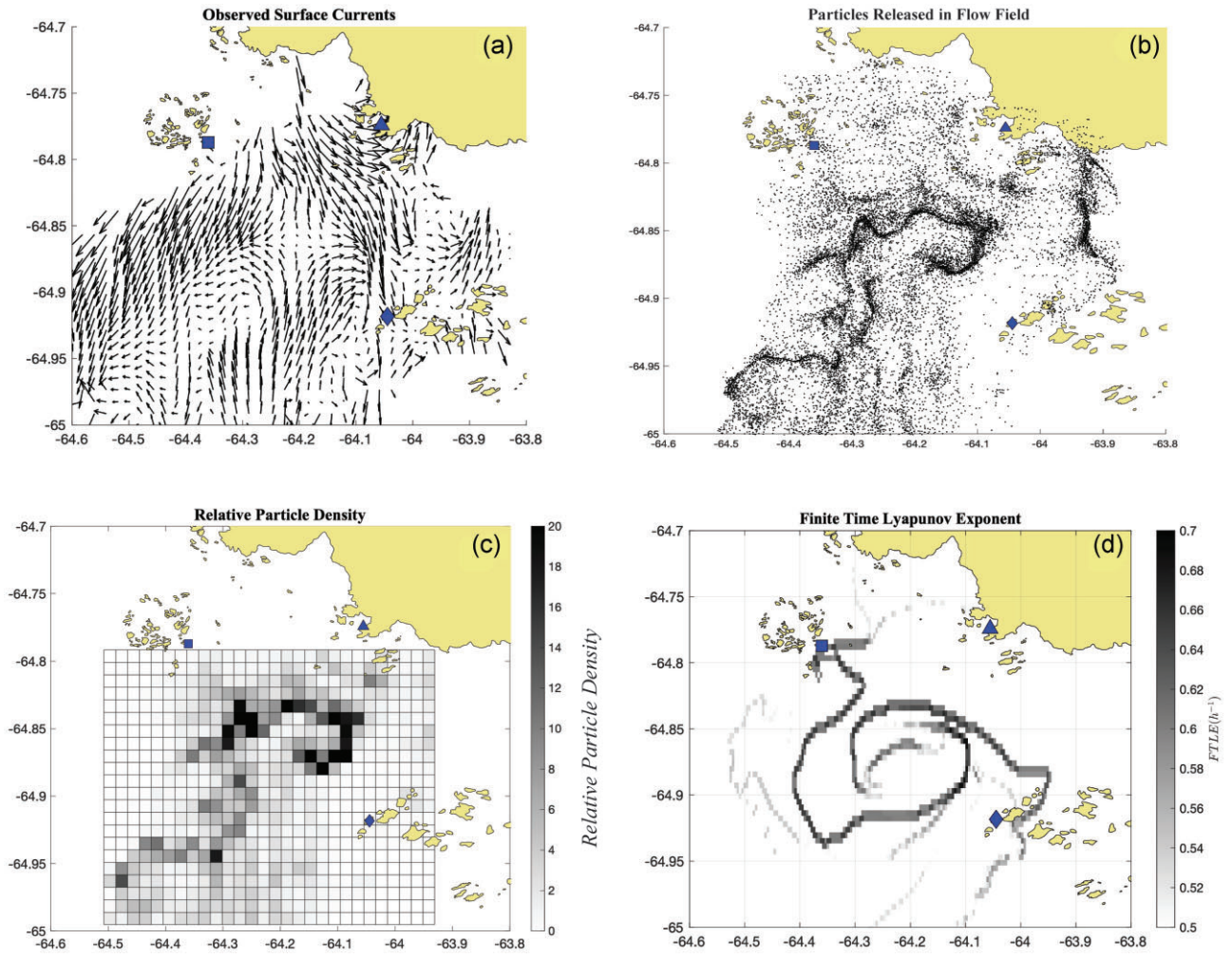

Figure 2 The HFR observed surface current velocity field (a), advected particles released following methods detailed in section, "RPD" (b), RPD, only positive values are shown (c), and FTLE (d) from 9th January 11:00 GMT over the study region. The three HFR stations are indicated with polygons. (© 2022 IEEE. Reprinted, with permission, from Veatch et al. (2022, preprint: not peer reviewed).

Autonomous glider

A Slocum glider was deployed in Palmer Deep Canyon from January to March 2020. Gliders are buoyancy driven autonomous vehicles that dive and climb through the water column in a "sawtooth" pattern. The glider used in this study was piloted to hold station at the head of Palmer Deep Canyon, profiling the same region throughout the season from the surface to 1000 m, just above the seafloor (Fig. 1). The glider sampled at a 0.25-m vertical resolution. Aboard the glider was a sensor suite that measured physical structure of the water column (CTD, Seabird), phytoplankton fluorescence and particle backscatter (Eco Triplet, Wet Labs), and krill biomass (Acoustic Zooplankton Fish Profiler, ASL Environmental Sciences).

Data from the stationary glider was profiled and MLD was calculated as the maximum buoyancy frequency following methods in (Carvalho et al. 2017), the same methodology used to determine MLD from the ACROBAT data. Similar to the ACROBAT, glider profiles were designated as "phytoplankton patches" if the particle backscatter integrated over the mixed layer was 5% higher than the daily median, adapted from Thomalla et al. (2015). These data were used in the calculation of the time-scale of phytoplankton patches detailed in section, "Determining integration time".

LCSs

Several LCS techniques have been applied to ocean systems in the past decade for their ability to quantify areas in ocean currents (or any velocity field) that exert an impact on nearby drifting particles (Haller 2015). Such areas are known as coherent structures. Coherent structures can identify local extrema of repulsion, attraction, and shearing of flow (Haller 2015). Attracting coherent structures will quantify the attraction of passive drifters in a flow field, or plankton in ocean currents (Shadden et al. 2005, Haller 2015).

In this study, LCS metrics from two distinct classes will be used to quantify physical advective features within the HFR observed surface current field: RPD, which have been used in Palmer Depp Canyon in previous studies (Oliver et al. 2019, Veatch et al. 2022) and FTLE, which have been used in a variety of open ocean ecological studies (Haller 2001, Huhn et al. 2012, St-Onge-Drouin et al. 2014, Fahlbusch et al. 2022, Veatch et al. 2022). This paper will suggest appropriate uses for both metrics dependent on available ecological observations, ensuring that the ecological community applies appropriate LCS techniques with an understanding of how these tools differ.

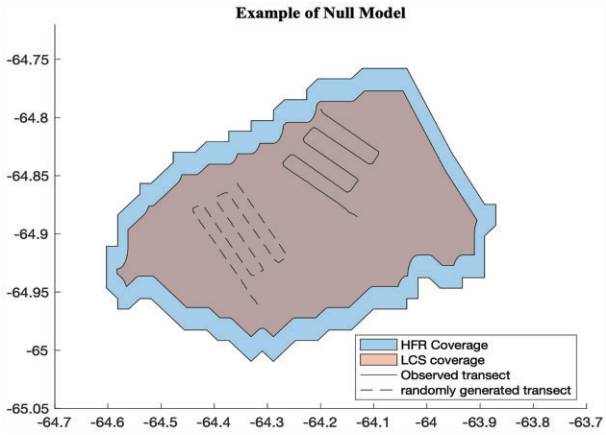

Figure 3 ACROBAT transect (solid line) and one randomly generated transect (dashed line) within the HFR coverage (larger shape) and LCS coverage (smaller shape) of the study region.

RPD

RPD reports the position of drifters at a single timestamp by normalizing the density of drifters within a gridded bin system in the study field. RPD calculations begin with releasing virtual particles over a regular grid and tracking them through a velocity field. RPD is then quantified by summing the number of drifters in each grid box, and normalizing by the median number of drifters in all grid boxes (Fig. 2c). New particles were released in a regular grid across the 80% coverage of the HFR footprint every 3 h. Particles were not counted until they had been advected in the velocity field for 6 h and were no longer counted when they were advected out of the HFR domain, or after they became three days old. The 6-h integration time is explained in section "Determining integration time". Given the average residence time of 2 days (Kohut et al. 2018), the 3-day threshold was chosen to coordinate with the time phytoplankton will spend in the surface layer of the study domain. This methodology follows that used by Oliver et al. (2019) and Veatch et al. (2022). Two dimensional HFR data is used to calculate RPD, relying on the assumption that the integrated surface divergence is zero, and no particles are lost from or added to the surface due to vertical velocities. Therefore, RPD will map the instantaneous concentration of surface associated particles across the entire domain given the evolving surface current fields provided by the HFR.

To negate artifacts in results caused by the edges of the HFR domain where particles entering or leaving the domain may be unaccounted for, the domain of RPD results used was smaller 3 km smaller than the domain of the inputted velocity field (Fig. 3). This is about how far the average particle travels over the integration time (6 h).

FTLE

FTLE use the horizontal separation distance between two particles relative to a fixed point over a defined time interval to quantify the strength of coherent structure (either repelling or attracting) at each point on a gridded velocity field. To calculate repelling FTLEs, a forward trajectory is used, and to calculate attracting FTLEs, a backward trajectory is used. In this study, attracting FTLEs were calculated. FTLE's ability to integrate over trajectories sets this technique apart from instantaneous separation rate (Okubo 1970, Weiss 1991) by introducing particle position "memory." Coherent structures are defined by the FTLE metric as ridges in the flow field where neighboring particles are converged toward, and then diverged along a ridge. The strengths of these ridges are quantified by the integrated attraction/separation rate between two particles (Fig. 2d).

FTLE calculations begin with a velocity field over some selected time. Finite differencing is then used over a defined auxiliary grid to numerically compute the derivative of the flow map. Next, the Cauchy–Green strain tensor field is computed from the derivative of the flow map as well as its eigenvalue field and eigenvector field. Then, the "stretching" of the field is computed as in (1), where $S(x_0)$ is the maximum stretching at point x_0, λ_i is the eigenvector field, and C is the Cauchy–Green strain tensor.

$$S(x_0) = [max_{i=1:N}\lambda_i(C(x_0))]^{1/2}. \quad (1)$$

FTLE is then computed with (2) over a finite time T (Dosio et al. 2005, Haller 2015, Haller et al. 2018).

$$FTLE(x_0, t_0, T) = \frac{1}{T}\ln(S(x_0)). \quad (2)$$

These calculations result in a time dependent FTLE field for every timestamp of inputted velocity data. In the case of this study, a map of FTLE was produced every hour for the two-and-a-half-month study period.

This relative motion between two neighboring particles and the inclusion of a rate of change component are the key ways in which the FTLE metric differs from the RPD metric. Like RPD, FTLE will vary over space and time when applied to a discrete set of velocity data. FTLE calculations (1 and 2) result in a material surface that then can be projected at a set resolution back onto the study region. FTLE results were projected at the resolution of the HFR (1 km) so as to not stretch the observations further than the input data should be able to resolve.

FTLE calculations were performed using a MATLAB software toolbox (Halleret al. 2015) that was modified for use on HFR data (Fig. 2d). To negate artifacts in results caused by the edges of the HFR domain where it may seem that particles suddenly stop or are lost, the domain of FTLE results used was smaller than the domain of the inputted velocity field. As with the RPD results, the domain was shrunk by 3 km (Fig. 3).

Determining integration time

In calculating FTLE results, varying integration time will identify transport features of different scales. As if fine tuning a microscope, features of a certain scale will come into focus as the integration time is adjusted. This study is interested in the scale of horizontal advective features that create ephemeral phytoplankton patches, therefore observations of phytoplankton patches and surface currents were used to determine the integration time of LCS calculations. To calculate the biological time-scale, the stationary glider was used (Fig. 1). Glider profiles were determined as observing a phytoplankton patch or not. Consecutive profiles of phytoplankton patches were considered to be from the same phytoplankton patch. The average time of consecutive phytoplankton patch profiles was determined to be the average time a phytoplankton patch remains in the same geographic location, 6.2 h, and therefore is the time-scale of the phytoplankton patches. To calculate the physical time-scale, the HFR observed surface currents were used. The autocorrelation of the HFR observed surface current velocities was calculated at each grid point in the HFR

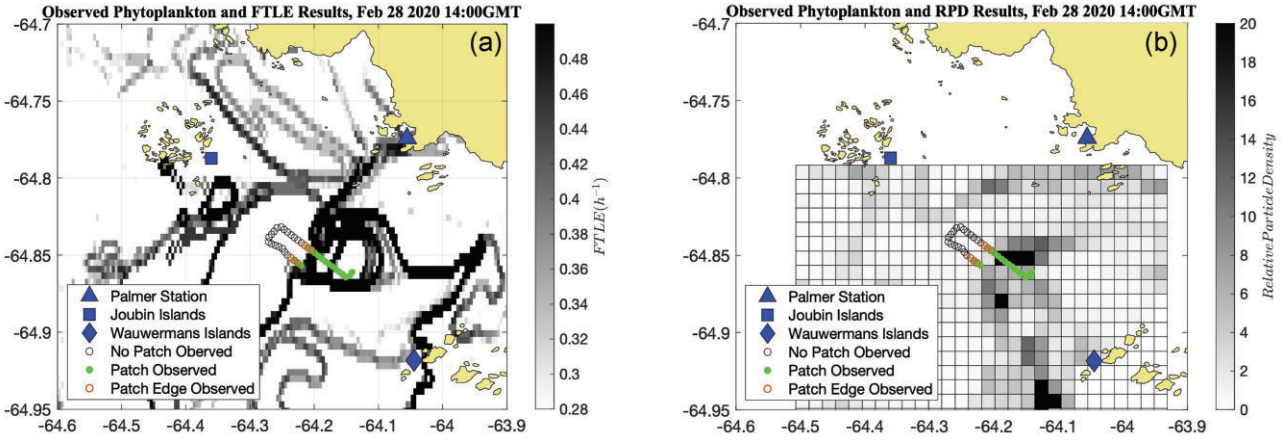

Figure 4 Example of LCS results plotted with 1 h of phytoplankton observations from the ACROBAT towed survey on 28th February at 14:00 GMT, (a) FTLE and (b) RPD.

field and normalized to variance. Autocorrelation was then averaged over each grid point of the same lag time. The time when the HFR observed surface current velocities decorrelated was defined as when the normalized autocorrelation function passed the e-fold scale: 5.5 h. This calculation was repeated with starting times during various stages of the tidal cycle and similar results were found each time. These results are shown in Fig. 3 of Veatch et al. (2022) and follow methods described therein.

The physical and biological timescales of Palmer Deep Canyon reflect the strength of tidal influence in the system. Recent studies have shown the effect of tides on surface ocean particle trajectories (St-Onge-Drouin et al. 2014, Gomez-Navarro et al. 2022) and the response of upper trophic creatures (Adélie penguins) to shifts in tidal regimes in Palmer Deep Canyon (Oliver et al. 2013). Therefore, the tidal cycle influence on particle dispersion, surface currents, and ecology in this system is consistent with these studies.

Based on this analysis, the integration time used for FTLE calculations was 6 h, which approximates the decorrelation time scales of phytoplankton patches and surface current velocities. In the calculation of RPD, particles were not counted in density calculations until 6 hours after their release. Unlike RPD, FTLE's integrate over the particle's trajectory in time, meaning the maps of FTLE results produced at a timestamp incorporate trajectory data from the previous 6 h.

Matching LCS results to phytoplankton patches

To compare the collocation of coherent structures and phytoplankton patches, results were matched in both space and time (Fig. 4). LCS results are space and time dependent, and produce mapped results every hour. The observation time of each phytoplankton patch was rounded to the nearest hour and compared to that hour's corresponding LCS field. Next, each ACROBAT profile was assigned an FTLE and RPD value from the nearest grid point to the ACROBAT profile's GPS location. The ACROBAT profile was always within 500 m of the nearest FTLE and RPD point, which are on 1 km grids. The FTLE and RPD values of all ACROBAT profiles within the same defined phytoplankton patch were averaged into a patch average value. The same was done for each defined patch edge. This resulted in each defined phytoplankton patch having one average patch center FTLE and RPD value and two average patch edge FTLE and RPD values. Phytoplankton patch definitions from the stationary glider were only used to calculate decorrelation scales and were not matched to LCS results to simplify the interpretation of results.

Creating a null model

To evaluate the performance of the LCS overlap with the observed plankton patches, a null model was created to represent a random distribution of patches. Within the bounds of the LCS results (Fig. 3), the ACROBAT transect was randomly rotated and translated along longitude, and randomly translated along latitude. A total of 100 random transects were created from each of the 16 survey days, culminating in 1600 randomly generated transects. The LCS values of each observed phytoplankton patch could then be compared to the LCS values of the 100 randomly generated versions of that patch. If LCS values of the observed patches were significantly greater than the LCS values of the 100 randomly generated versions of those patches, passing a one-sided Wilcoxon rank-sum test, then it was concluded that the observed patches were collocated with a strong LCS. To visualize the difference between observed and randomly generated patch LCS values, the difference was taken between each observed patch LCS value and the average of the corresponding 100 randomly generated patches. This was done for patch centers and patch edges.

Results

Throughout the 16 ACROBAT surveys, 40 distinct phytoplankton patches and 80 phytoplankton patch edges profiles were observed. These data were used to test the collocation of phytoplankton patches in space and time with our two LCS metrics (FTLE and RPD; Fig. 4).

RPD collocated with phytoplankton patches

RPD values had little difference between phytoplankton patches observed by the ACROBAT and randomly generated phytoplankton patches (Fig. 5a). The distributions of observed and randomly generated phytoplankton patch centers failed a one-sided Wilcoxon rank-sum test ($P = .8458$) indicating that the RPD values of the null model (randomly generated patch centers) are not significantly less than the RPD values of the observed phytoplankton patch centers. The distributions of

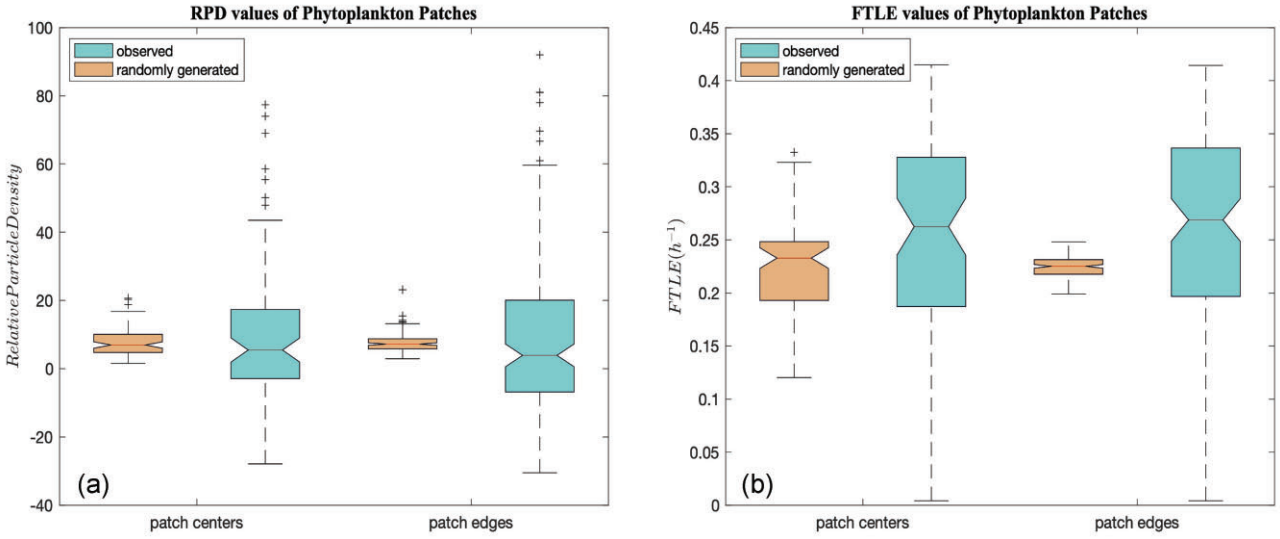

Figure 5 Box and whisker plots of RPD values (a) and FTLE values (b) of phytoplankton patch centers and phytoplankton patch edges of observed (teal) and randomly generated (orange) phytoplankton patches. Boxes represent the interquartile range, whiskers represent the data range, outliers are plotted as +, the median of the data is shown with a horizontal line, and notches represent the confidence interval for the median.

observed and randomly generated phytoplankton patch edges also failed a one-sided Wilcoxon rank-sum test ($P = .9941$) indicating that the RPD values of the null model (randomly generated patch edges) are not significantly less than the RPD values of the observed phytoplankton patch edges.

The distribution of RPD is shifted slightly above zero. Although RPD is a relative amount, this was expected because the edges of the RPD were not used (section "FTLE", Fig. 3), negating the likely low RPD values right at the edge of the HFR domain.

FTLE collocated with phytoplankton patches

The FTLE values of observed phytoplankton patches were higher than the randomly generated null model (Fig. 5b). The distributions of observed and randomly generated phytoplankton patch centers passed a one-sided Wilcoxon rank-sum test ($P = .0034$) indicating that the FTLE values of the null model (randomly generated patch centers) are significantly lower than the FTLE values of the observed phytoplankton patch centers. The distributions of observed and randomly generated phytoplankton patch edges also passed a one-sided Wilcoxon rank-sum test ($P = 4.6017 \times 10^{-6}$) indicating that the FTLE values of the null model (randomly generated patch edges) are significantly lower than the FTLE values of the observed phytoplankton patch edges. In Fig. 6, the distribution of results is mostly positive, indicating that for most patch centers and patch edges the randomly generated "background" FTLE values were less than the observed patch FTLE values. This signal was slightly stronger in patch edges than patch centers for all surveys, although this difference was not significant (one-sided Wilcoxon rank-sum test, $P = .2661$). This pattern holds when the phytoplankton center and edge data are combined and compared to the combined null model values, with the observed data having greater FTLE values with statistical significance (one-sided Wilcoxon rank-sum test, $P = 1.1892 \times 10^{-7}$).

Differences between observed and randomly generated FTLE patch center and patch edge values were separated into "stratified surveys" and "mixed surveys." The difference between observed and randomly generated patch center FTLE values for stratified surveys and mixed surveys are significantly different (one-sided Wilcoxon rank-sum test, $P = .0230$) with higher FTLE values on stratified days. The same pattern holds for patch edges, with the difference between observed and randomly generated patch edges on stratified days having significantly higher FTLE value differences than those on mixed days (one-sided Wilcoxon rank-sum test, $P = .0013$) (Fig. 6).

Case studies of FTLE on stratified and mixed days

To better understand these results, four case study survey days were examined. They were designated as stratified well performing, mixed well performing, mixed poor performing, and stratified poor performing (Fig. 7). Stratified, well performing survey days such as 3rd March had long, thin FTLE structures that persisted for multiple hours (Fig. 7a). The ACROBAT observed phytoplankton patches on these narrow, persistent structures and observed no phytoplankton patches when the survey left these structures. 3rd March also had an average maximum particle backscatter depth of 2.72 m, meaning that most phytoplankton patches were close to the surface within the region where the HFR sampling is most accurate. This is in contrast with the mixed, well-performing survey days such as 28th January which had round, short FTLE structures (Fig. 7b) and an average maximum particle backscatter depth of 17.07 m. On survey days when large amounts of phytoplankton were observed, such as 28th January, there was enough phytoplankton to fill the wider round structures more typical of mixed days and the phytoplankton patches were observed within the FTLE structures. This is shown in Fig. 8(b) where the 28th January survey has many occurrences of high particle backscatter, similar to the 3rd March survey. It was concluded that an abundance of large phytoplankton patches is an important prerequisite to a mixed survey having well-performing FTLE.

Mixed, poor-performing survey days such as 21st February had very few FTLE structures within the survey region (Fig. 7d). Compared to the other three case study days, 21st

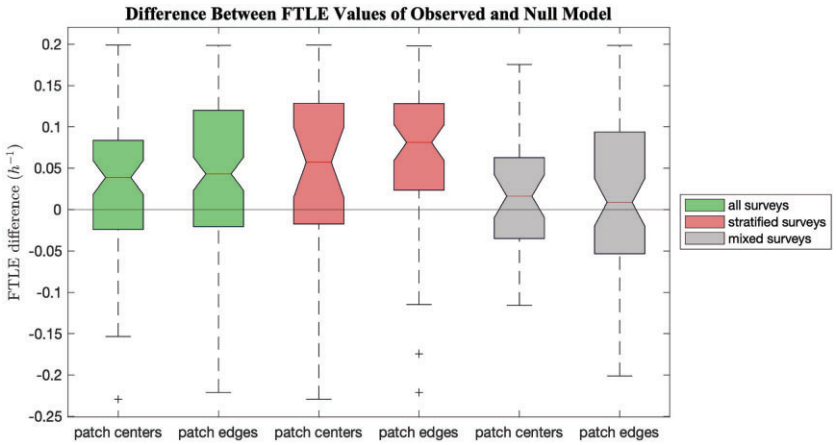

Figure 6 Box and whisker plots of the difference between FTLE values of observed phytoplankton patch centers and edges and randomly generated patch centers and edges of all surveys (left two box and whiskers), stratified surveys (middle two box and whiskers), and mixed surveys (right two box and whiskers). The horizontal line at zero difference separates the well-performing FTLE and patch matches above the line, and poor performing FTLE and patch matches below the line. Boxes represent the interquartile range, whiskers represent the data range, outliers are plotted as +, the median of the data is shown with a horizontal line, and notches represent the confidence interval for the median.

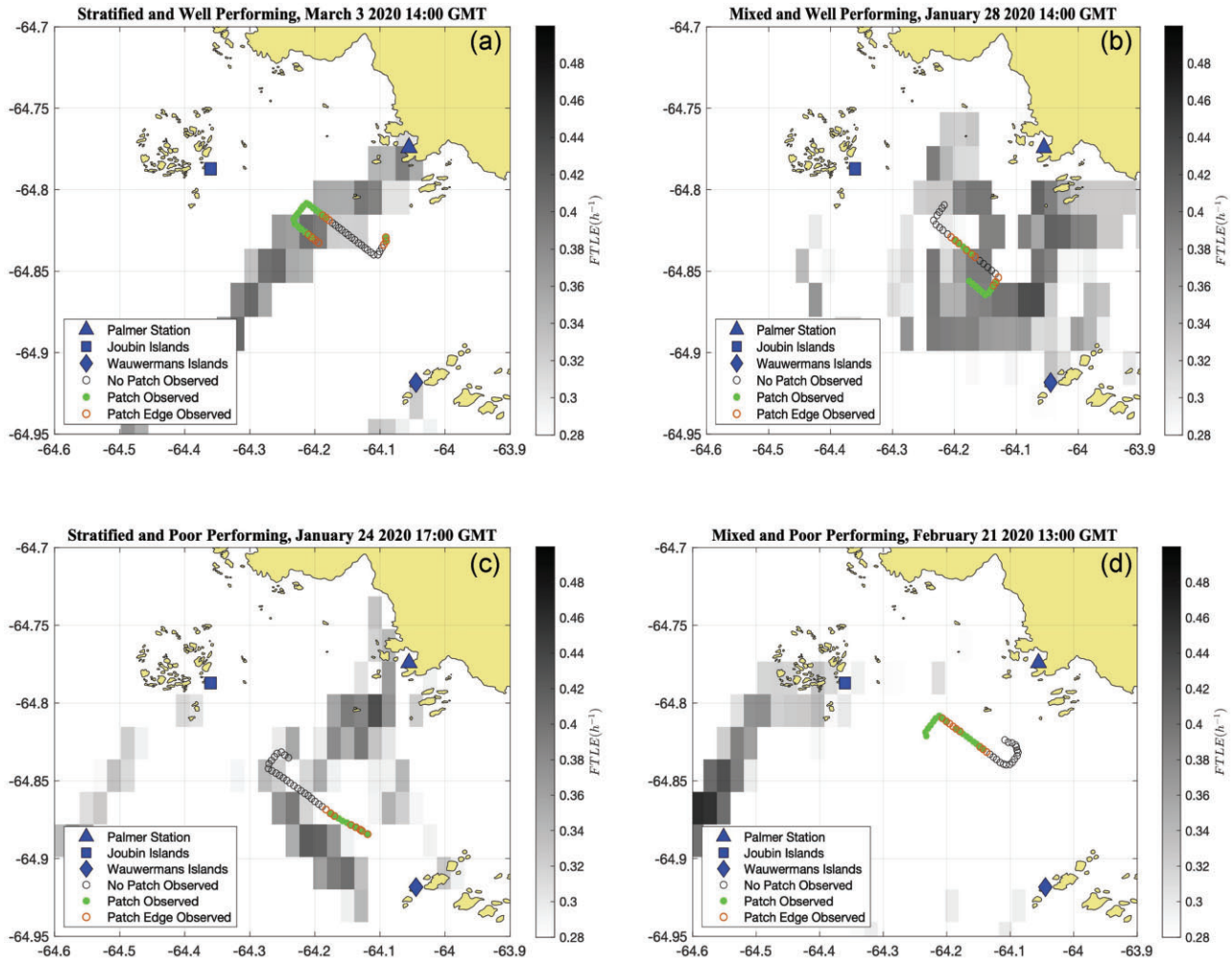

Figure 7 Four case study days of ACROBAT observed patch centers (filled circles) and patch edges scattered over FTLE results. Stratified day with high correlation between high FTLE values and phytoplankton patches (a), mixed day with high correlation between high FTLE values and phytoplankton patches (b), stratified day with low correlation between high FTLE values and phytoplankton patches (c), and mixed day with low correlation between high FTLE and high values and phytoplankton patches (d).

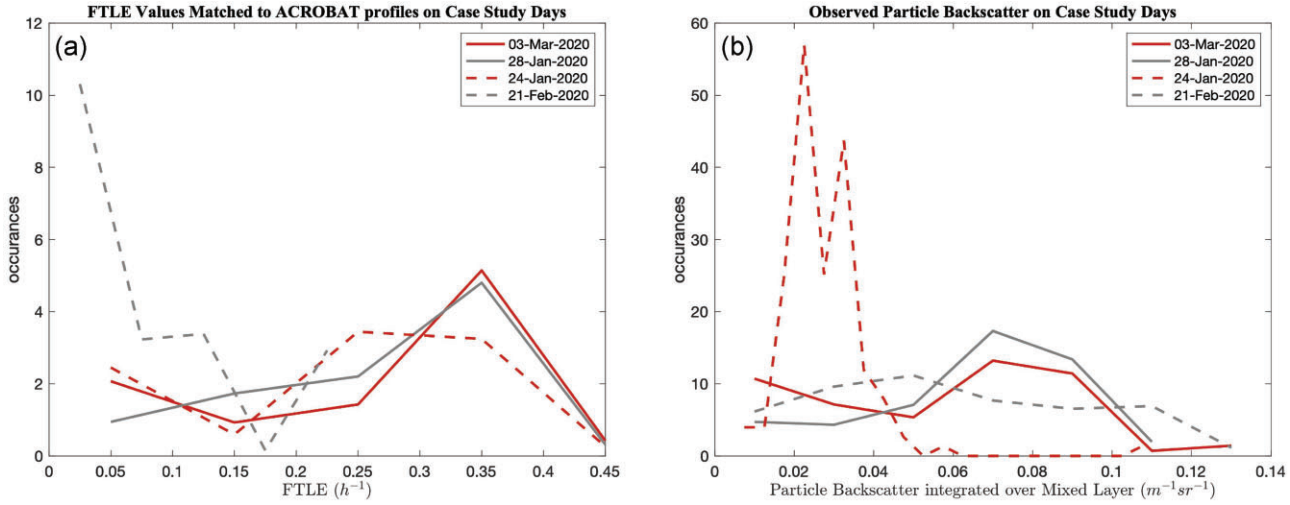

Figure 8 Histogram of (a) FTLE values matched in space and time with each ACROBAT profile observed during the four case study survey days in Fig. 6 and (b) particle backscatter observed by the ACROBAT integrated for each profile to the MLD of the four case study survey days shown in Fig. 7.

February had many observations of low FTLE values (Fig. 8a). It is important to remember that due to the nature of our definition of "phytoplankton patch" normalized to the survey day, there will always be phytoplankton patches defined in a given survey, even if there are no strong FTLE features. It was concluded that the lack of defined FTLE features was the reason this survey day had few phytoplankton patches collocated with FTLE defined attracting features.

Stratified, poor performing survey days such as 24th January were expected to perform well due to well-defined surface layers and shallow phytoplankton patches (Fig. 7c). In the case of the 24th January survey, it is suspected that low abundances of phytoplankton were the cause of the FTLE results' poor performance. In a histogram of integrated mixed layer particle backscatter (the proxy used to define "phytoplankton patches") observed during the ACROBAT surveys of our four case study days, 24th January has a high occurrence of low mixed layer particle backscatter measurements (Fig. 8b). Figure 8(b) suggests that the phytoplankton during the 24th January survey were diffuse across the study region, with many observations of low particle backscatter. Low phytoplankton levels could be because Palmer Deep Canyon had lower abundances of phytoplankton that day, or because our ACROBAT survey transect missed the FTLE features that were concentrating large amounts of phytoplankton. Again, due to the nature of our definition of phytoplankton patch, there were "patches" defined even though phytoplankton observations were overall of low concentration. Many observations of low phytoplankton suggests that the phytoplankton are not well concentrated, but diffuse throughout the study region. On days when there are no attracting features or when the ACROBAT survey does not encounter any attracting features, this is expected. In contrast, the well-performing days have many occurrences of high phytoplankton, suggesting that there is enough phytoplankton biomass to be concentrated into distinct patches.

The poorer performance of FTLE on some survey days could be due to inhomogeneous currents in the surface layer, a lack of large phytoplankton patches on mixed days, a lack of strong attracting physical features, or likely some combination of these three. These four case studies demonstrate that FTLE ridges tend to be narrower and more filament-like on stratified surveys and wider on well-mixed surveys, and that surveys with low amounts of phytoplankton or FTLE do not show phytoplankton patches to align as often with higher FTLE values than surveys that have high amounts.

Discussion

Concentration of sparse food sources into discrete patches is an important mechanism for the maintenance of coastal biological hotspots such as that in Palmer Deep Canyon. Using Palmer Deep Canyon as a natural laboratory, this investigation has determined the importance of physical advection in the distribution of plankton patches at the very base of the food web. LCS metrics, when applied carefully, can be used as tools to elucidate the role of advective transport in complex coastal regions. In this study, FTLE expounds the relationship between HFR observed surface currents and phytoplankton patch location. The difference between single particle tracking methods like RPD and paired particle tracking like FTLE provides a roadmap for when each metric is appropriate to apply to coastal ecosystems.

Two-dimensional assumptions in LCSs

The use of LCS allows for the identification of ocean features that cannot be seen from velocity fields alone. LCS applied to ocean currents have the capacity to quantify underlying patterns in fluid trajectories that potentially concentrate marine resources in the ocean. However, there are limitations to these LCS, which must be thoroughly understood to properly apply metrics and interpret results. LCS must have the same dimensionality as their input. In this study, two-dimensional velocity data from three HFRs were used to calculate LCS, constraining resulting LCS to two dimensions at the ocean surface. Additionally, HFRs observe surface flow while phytoplankton patches can exist at variable depths. Below we explore the implications of two-dimensional LCS in coastal regions and the depth of HFR measurements, demonstrating that these limitations do not impede this study's ability to quantify phytoplankton concentrating features.

Pelagic, open ocean regions that are dictated largely by geostrophic, two-dimensional flow have been the subject of past studies using LCS to identify patterns of phytoplankton transport (Lehahn et al. 2007, Hernández-Carrasco et al. 2011, Huhn et al. 2012, Li et al. 2015, Lévy et al. 2018, Liu et al. 2018). In contrast, coastal regions are complicated by vertical velocities creating a three-dimensional flow field. Vertical velocities in our study region, Palmer Deep Canyon, are small compared to horizontal surface flow, especially given the short residence time of the region. With an average residence time of 2 days (Kohut et al. 2018) and an average vertical velocity magnitude of 2.84×10^{-5} ms^{-1} between January and March (calculated from divergence in HFR), a free drifting particle in Palmer Deep Canyon experiences on average 4.9 m of vertical displacement during its ∼2 day residency in the system. This average vertical displacement of 4.9 m is within the average surface MLD of ∼20 m. Consequently, it is reasonable to accept the two-dimensional LCS assumptions. Previous work has shown LCS in the open ocean associated with relatively strong vertical velocities at fronts (Mathur et al. 2019, Siegelman et al. 2020). In Palmer Deep Canyon, maximum vertical velocities are around 0.405×10^{-3} ms^{-1}, which is an order of magnitude smaller than maximum vertical velocities found at open ocean LCS by Siegelman et al. (2020) of 1.15×10^{-3} ms^{-1} at fronts. Whereas LCS in the open ocean can last for days, LCS in Palmer Deep Canyon have a lifespan on 5 h on average, which is when the autocorrelation function of FTLE results pass the e-folding scale, on average throughout the study domain and season. Vertical velocities associated with LCS in Palmer Deep Canyon are likely smaller due to the short lifespan of these features.

There could be small vertical velocities not detected by the 1 km resolution of the HFR data, likely more present on survey days designated as "mixed." These vertical velocities although small in spatial scale may be large in magnitude, and are more likely within strong gradients associated with density fronts. Such vertical velocities could have an impact on phytoplankton (Mahadevan 2016). Our dataset cannot resolve these vertical velocities, exposing a limitation of the data rather than of the two-dimensional assumption of the LCS metrics.

HFR measurements observed only the horizontal surface layer of the flow (Stewart and Joy 1974, Paduan and Graber 1997). For the HFR frequencies deployed in Palmer Deep the surface measurement is within the upper 2 m of the water column. When the mixed layer is completely homogeneous, these measurements can be extrapolated to represent the whole mixed layer. Use of HFR to calculate LCS has had some success in previous studies (Shadden et al. 2009, Hernández-Carrasco et al. 2018, Fahlbusch et al. 2022, Veatch et al. 2022) extrapolating HFR data to represent the whole mixed layer. In this study, phytoplankton patches were defined by ACROBAT observed profiles integrated to the observed MLD. The sensitivity of the integration depth to patch definition was evaluated and described in greater detail in Supplementary material S3. This analysis repeated patch definition with a constant integration depth of 5 m, which is closer to the effective depth of the HFR measurements (Stewart and Joy 1974) than most MLDs (average MLD is 20.8 m). However, the same patterns were found with both integration depths (Figures S2 and S3), showing that the depth of integration (constant 5 m or variable mixed layer) did not affect our conclusions.

Further, the physical and biological timescales of Palmer Deep Canyon are ∼6 h, within 1 h of each other, which is within the time resolution that we expect the HFR and glider data (Fig. 1) to observe. Matching physical and biological time-scales indicates that both the surface currents and the phytoplankton patches are changing at the same rate, suggesting that the main driver of change in phytoplankton patch location is advection resolved by the HFR observed surface currents. This provides further confidence that LCS can quantify a major mechanism of phytoplankton patch formation in Palmer Deep Canyon.

Phytoplankton patch collocation with FTLE and RPD

LCS values of observed patches in comparison to the null model (the randomly generated patches) suggest that higher values of FTLE results collocate with phytoplankton patches more often than higher values of RPD results (Fig. 5). In assessing this result, it is important to note that the two LCS metrics differ in several ways including single particle (RPD) vs. pair of particles tracking (FTLE), FTLE's ability to incorporate rate of change, and FTLE's flexible integration times.

The fact that FTLE often collocate with phytoplankton patches in Palmer Deep Canyon suggests that phytoplankton are acting as free drifters in the surface layer. So then, why do the particle trajectories of the RPD metric, which is designed to track the accumulation of surface drifters, do such a poor job of collocating with phytoplankton patches? Let us begin with considering cases when simple particle trajectories (RPD) are useful for tracking free drifters. Seeding particles where drifters are observed and running a trajectory backwards in time will track the source of those drifters, or when the source is known, such as in an oil spill, particles released at the observed source will track where those drifters accumulate. However, in this study we seek to identify areas in the HFR observed surface current field that have stronger attracting mechanisms than elsewhere in the field, without any added information about the source or location of drifters (phytoplankton) in the LCS calculations. In this case, LCS calculated from relative positions of pairs of particles characterize these areas of attraction independent of particle initial position, and dependent on the integrated backwards trajectories of those particles. This concludes that simple particle trajectories (RPD) are useful when the source or destination and relative abundance of plankton is known, so particle releases can be catered to location and density. FLTE are useful when the source or destination is unknown and the entire flow field is searched for attracting features. While single particle trajectory methods such as RPD use simpler calculations, these results suggest that ecologists should take the time to use more complex, paired particle tracking such as FTLE when investigating the role of physical advection in the spatial ecology of phytoplankton.

Where RPD only accounts for the location of the drifters at one timestep, FTLE accounts for the velocity of the drifters relative to other drifters, introducing a rate of change consideration into the quantification of attraction (Haller 2015). The rate of change (velocity) used in FTLE calculations incorporates additional information that the location-based calculations in RPD do not. Additionally, FTLE integrate over particle trajectories giving each calculation a "memory" of the inputted integration time (6 h in this case, section "Determining integration time") (Haller 2015). Application of FTLE allows

for the scale of the features that are transporting and concentrating plankton in Palmer Deep Canyon to be elucidated (St-Onge-Drouin et al. 2014). The ability to determine this integration time allowed us to calculate FTLEs that identified the scale of feature that we knew to be important in the system from our analysis. Both rate of change and integration considerations could contribute to their better performance, diagnosing the underlying flow responsible for transport rather than following the flow field as the RPD analysis does. Such flexibility in FTLE calculations could make FTLE a powerful tool in coastal systems when working with submesoscale features on subtidal scales and highly variable nonlinear flow. Therefore, the improved performance of FTLE over RPD in aligning with observed phytoplankton patches suggests that processes that overlap with patches are best identified by the attraction of paired particles, not the absolute concentration of a field of released particles.

It should be noted that this study does not account for biological mechanisms of phytoplankton concentration, such as grazing pressure or growth. Because the growth period of phytoplankton is greater than the residence time in Palmer Deep Canyon, growth rate was not considered (Kohut et al. 2018). This study also assumes that phytoplankton are not limiting in Palmer Deep Canyon, meaning grazing pressure would not have a large effect on results.

FTLE performance on patch centers and patch edges during stratified and mixed conditions

For each survey, we mapped both phytoplankton patch centers and edges to investigate if each LCS metric better aligned with specific regions of the patches. It was originally hypothesized that RPD would better align with patch centers while FTLE would better align with patch edges because the FTLE paired particle metric better characterizes boundaries between distinct modes of flow (Haller 2015) while RPD characterize a concentration of drifters (Oliver et al. 2019). The distinction between patch centers and patch edges investigates whether different transport mechanisms determine where the center of attraction (the patch center) vs. the extent or cut-off point of the phytoplankton patch. FTLE performed slightly better on patch edges than patch centers. This could be because the areas where particles diverge along a ridge, categorized by FTLE as strong coherent structures, separate water with different phytoplankton levels. However, in this study the distribution of edge and center FTLE values were not significantly different. If there is a difference between edge and center it is likely that we would need to have a higher sample size to detect it.

FTLE collocated with phytoplankton patches more often on stratified surveys than mixed surveys (Fig. 6). Stratification in the upper water column will change the complexity of the surface flows over our study site. When the upper water column is strongly stratified, the surface layer will flow more independently of the subsurface, with little exchange between the two layers, setting up two-dimensional flow in the surface layer. Mixed conditions are more indicative of the surface and subsurface layers exchanging physical properties through vertical mixing. It was originally hypothesized that LCS would not perform well on a well-mixed water column because vertical velocities would invalidate the two-dimensional assumption of LCS. However, it was found that the vertical velocities in Palmer Deep Canyon were negligible at the studied scales. Additionally, there was little difference between the vertical velocities over the ACROBAT survey on survey days that were determined as mixed and those that were determined as stratified, 3.47×10^{-5} m s^{-1} for mixed days and 3.60×10^{-5} m s^{-1} for stratified days. This suggests that the better alignment of FTLE and phytoplankton patches on stratified surveys was due to (1) homogeneous and inhomogeneous mixed layers or (2) a biological response in the way phytoplankton patches are formed on mixed surveys.

A mixed water column with a deep MLD may be indicative slight differences in ocean velocities between the surface and bottom of the mixed layer. Although these mixed layers pass the definition of a mixed layer (Carvalho et al. 2017), the surface waters where the HFR is observing the flow may be different than a few meters below the surface, still in the mixed layer, where the phytoplankton are experiencing the flow. This would mean that on mixed days the HFR is less representative of the currents that are concentrating the phytoplankton patches.

The four most mixed (smallest difference in density between the surface and 50 m) surveys had an average depth of maximum particle backscatter (the proxy used to define phytoplankton patches) of 11.80 m with a standard deviation of 15.05 m, well below the few meters the HFR can safely observe. The four most stratified surveys had an average depth of maximum particle backscatter of 2.97 m with a standard deviation of 1.98 m. This implies that on mixed days, where the mixed layer may be less uniform, the phytoplankton patches are deeper in the mixed layer and are likely experiencing ocean currents that are not well resolved by the HFR data. Therefore, the poorer match between FTLE and phytoplankton patches on mixed days is likely due to a limitation in observed data rather than a limitation in the dimensionality of the FTLE. However, even on well-mixed survey days, FTLE still often collocated with phytoplankton patches (Fig. 6), just not as often as they did on stratified surveys.

Conclusion

Our analysis indicates that HFR derived FTLE can be used to identify concentrating mechanisms in biological hotspots with complex submesoscale flows, validating their use in coastal systems (Fig. 5). Comparing the single particle tracking metric (RPD) with the paired particle tracking metric (FTLE) provided a mechanistic understanding of how surface currents in Palmer Deep Canyon are transporting and locally concentrating phytoplankton. The paired particle tracking metric (FTLE) more often identified areas of the flow field where phytoplankton were being concentrated into patches. FTLE's ability to incorporate rate of change, flexible integration times, and consideration of relative distance rather than final position allowed this metric to better capture the transport of phytoplankton.

FTLE does a slightly better job at identifying phytoplankton patch edges than centers, characterizing separatrices in ocean currents that separate different ocean flow patterns as well as high phytoplankton from low phytoplankton areas (Fig. 6). However, the difference between patch edges and patch centers was not significant, meaning that phytoplankton patch edges and patch centers both collocate with FTLE-identified coherent structures, and therefore are likely maintained by the same advective mechanisms. It was also concluded that the FTLE metric performs best when the water

column is stratified, which is indicative of vertical velocities and heterogeneity in the mixed layer being at a minimum, and phytoplankton patches closer to the surface within the sampling domain of the HFR. This is when the two-dimensional assumption of the FTLE calculations is the most accurate and the phytoplankton patches are closer to the surface enabling the HFR data to best measure the flow that the colocated phytoplankton are experiencing (Fig. 6). FTLE collocate with phytoplankton patches more often when the system has a substantial amount of strong coherent structures (Fig. 8a) and phytoplankton (Fig. 8b), meaning there are physical features present to concentrate the phytoplankton and there are large enough phytoplankton patches to fill the coherent structures.

The novelty of this study's application of LCS lies in the scale at which these metrics are applied, looking for structures that organize plankton dispersion on the order of hours within a few kilometers. This is the scale of the ocean at which the krill and the forage fish are interacting with ocean flows as they swarm, creating the prey availability central place foraging penguins rely on in Palmer Deep Canyon (Oliver et al. 2019). Results solidify the role of physical advection in the concentration of phytoplankton patches in Palmer Deep Canyon on these short time-scales, suggesting this area is sustained by delivery of phytoplankton through advection rather than local growth.

Further investigation of FTLE applied to coastal biological hotspots could inform ecosystem models by predicting bioactivity from ocean currents. Findings will also broaden the use of HFR data to locate areas of food web focusing, furthering our understanding of how coastal biological hotspots are maintained.

Acknowledgements

Many thanks to the Antarctic Support Contractor and their teams aboard the ARSV Laurence M. Gould, at Palmer Station, and headquarters in Denver, CO without whom a study of this scale would not be possible. Thank you to the students, postdoctoral scholars, and field assistants for their valued involvement in the SWARM project, in particular Ashley Hann, Dr Katherine Gallagher, Dr Jerome Pinti, Dr Thilo Klenz, Ethan Handel, and Jordi Maisch. We thank the Palmer Long-Term Ecological Research team and the Commission for the Conservation of Antarctic Marine Living Resources, for their advice and collaboration.

Supplementary material

The following Supplementary material is available at *ICES JMS* online. Supplementary material provides an explanation of methodology used to determine the low reencounter rate of phytoplankton patches on the ACROBAT towed survey mentioned in section "ACROBAT towed surveys". Details on the methodology for determining "stratified" and "unstratified" survey days (Figure S1) are also included. Last is the inclusion of a repeated analysis with a different definition of phytoplankton patch, integrating to a constant 5 m instead of the mixed layer depth (Figures S2 and S3), i.e. mentioned in Section "Two-dimensional assumptions in LCSs".

Conflict of interest: The authors have no conflicts of interest to declare.

Funding

This project is funded through the National Science Foundation, award number: 1745009.

Data availability

Data and code used in this study are publicly available on NSF funded project SWARM's BCO-DMO site and GitHub. High Frequency Radar observed surface currents are available in the gap-filled version used in this study on BCO-DMO (https://www.bco-dmo.org/dataset/917884). Code used to gap-fill these data are available on GitHub (https://github.com/JackieVeatch/SWARM_CODAR). Lagrangian Coherent Structure Results for both FTLE and RPD metrics are available on BCO-DMO (https://www.bco-dmo.org/dataset/917914, https://www.bco-dmo.org/dataset/917926) and the code used to produce these results can be found on GitHub (https://github.com/JackieVeatch/SWARM_LCS). The code was modified from open-source MATLAB library (Haller et al. 2015) for use on HFR data. ACROBAT data used to map phytoplankton can be found on BCO-DMO (https://www.bco-dmo.org/dataset/916046) and the code used to identify phytoplankton patches can be found on GitHub (https://github.com/JackieVeatch/SWARM_ACROBAT). Initial processing of the data was done with an open-source MATLAB library (Reister 2023). Glider data used to calculate the biological time-scale can be found on Erddap (https://slocum-data.marine.rutgers.edu/erddap/tabledap/ru32-20200111T1444-profile-sci-delayed.html) and the code used to calculate the biological and physical time-scales can be found on GitHub (https://github.com/JackieVeatch/SWARM_scales). All other code for analysis can be found on GitHub (https://github.com/JackieVeatch/SWARM_analysis). Any questions can be directed to Jacquelyn Veatch (jveatch@marine.rutgers.edu).

Author contributions

Jacquelyn M. Veatch, Josh T. Kohut, Matthew J. Oliver, Hank Statscewich, and Erick Fredj.

References

Abrahms B, Scales KL, Hazen EL *et al.* Mesoscale activity facilitates energy gain in a top predator. *Proc R Soc B Biol Sci* 2018;**285**:20181101. https://doi.org/10.1098/rspb.2018.1101.

Barrick DE, Evans MW, Weber BL. Ocean surface currents mapped by radar. *Science* 1977;**198**:138–44. https://doi.org/10.1126/science.198.4313.138.

Benoit-Bird KJ. Resource patchiness as a resolution to the food paradox in the sea. *Am Nat* 2023;**203**:1–13.

Carvalho F, Fitzsimmons JN, Couto N *et al.* Testing the Canyon Hypothesis: evaluating light and nutrient controls of phytoplankton growth in penguin foraging hotspots along the West Antarctic Peninsula. *Limnol Oceanogr* 2020;**65**:455–70. https://doi.org/10.1002/lno.11313.

Carvalho F, Kohut J, Oliver MJ *et al.* Defining the ecologically relevant mixed-layer depth for Antarctica's coastal seas. *Geophys Res Lett* 2017;**44**:338–45. https://doi.org/10.1002/2016GL071205.

Carvalho F, Kohut J, Oliver MJ *et al.* Mixing and phytoplankton dynamics in a submarine canyon in the West Antarctic Peninsula. *J Geophys Res Oceans* 2016;**121**:5069–83. https://doi.org/10.1002/2016JC011650.

Cotté C, d'Ovidio F, Chaigneau A *et al.* Scale-dependent interactions of Mediterranean whales with marine dynamics. *Limnol Oceanogr* 2011;**56**:219–32. https://doi.org/10.4319/lo.2011.56.1.0219.

Della Penna A, De Monte S, Kestenare E *et al.* Quasi-planktonic behavior of foraging top marine predators. *Sci Rep* 2015;**5**:18063. https://doi.org/10.1038/srep18063.

Dosio A, Vilà-Guerau de Arellano J, Holtslag AAM *et al.* Relating Eulerian and Lagrangian statistics for the turbulent dispersion in the atmospheric convective boundary layer. *J Atmospheric Sci* 2005;**62**:1175–91. https://doi.org/10.1175/JAS3393.1.

Emslie SD, Fraser W, Smith RC *et al.* Abandoned penguin colonies and environmental change in the Palmer Station area, Anvers Island, Antarctic Peninsula. *Antarct Sci* 1998;**10**:257–68. https://doi.org/10.1017/S0954102098000352.

Fahlbusch JA, Czapanskiy MF, Calambokidis J *et al.* Blue whales increase feeding rates at fine-scale ocean features. *Proc R Soc B Biol Sci* 2022;**289**:20221180. https://doi.org/10.1098/rspb.2022.1180.

Farazmand M, Haller G. Attracting and repelling Lagrangian coherent structures from a single computation. *Chaos Interdisc J Nonlinear Sci* 2013;**23**:023101. https://doi.org/10.1063/1.4800210.

Farazmand M, Haller G. Computing Lagrangian coherent structures from their variational theory. *Chaos Interdisc J Nonlinear Sci* 2012;**22**:013128–12. https://doi.org/10.1063/1.3690153.

Fraser WR, Trivelpiece WZ. *Factors Controlling the Distribution of Seabirds: Winter-Summer Heterogeneity in the Distribution of AdéLie Penguin Populations*. Washington: American Geophysical Union, 1996, 257–72.

Fredj E, Roarty H, Kohut J *et al.* Gap filling of the coastal ocean surface currents from HFR data: application to the Mid-Atlantic Bight HFR Network. *J Atmos Oceanic Technol* 2016;**33**:1097–111. https://doi.org/10.1175/JTECH-D-15-0056.1.

Genin A. Bio-physical coupling in the formation of zooplankton and fish aggregations over abrupt topographies. *J Mar Syst* 2004;**50**:3–20. https://doi.org/10.1016/j.jmarsys.2003.10.008.

Gomez-Navarro L, Van Sebille E, Morales Márquez V *et al.* The effect of model tidal forcing on virtual particle dispersion and accumulation at the ocean surface. *ESS Open Archive* 2023. https://doi.org/10.1002/essoar.10512397.3

Haller G. Distinguished material surfaces and coherent structures in three-dimensional fluid flows. *Phys D* 2001;**149**:248–77. https://doi.org/10.1016/S0167-2789(00)00199-8.

Haller G. Lagrangian coherent structures. *Annu Rev Fluid Mech* 2015;**47**:137–62. https://doi.org/10.1146/annurev-fluid-010313-141322.

Haller G, Beron-Vera FJ. Coherent Lagrangian vortices: the black holes of turbulence. *J Fluid Mech* 2013;**731**. https://doi.org/10.1017/jfm.2013.391.

Haller G, Beron-Vera FJ. Geodesic theory of transport barriers in two-dimensional flows. *Phys D* 2012;**241**:1680–702. https://doi.org/10.1016/j.physd.2012.06.012.

Haller G, Karrasch D, Kogelbauer F. Material barriers to diffusive and stochastic transport. *Proc Natl Acad Sci* 2018;**115**:9074–9. https://doi.org/10.1073/pnas.1720177115.

Haller G, Huhn F, Onu K. LCS tool: a computational platform for Lagrangian coherent structures. *J Comput Sci* 2015;**7**:26–36.

Hernández-Carrasco I, López C, Hernández-García E *et al.* How reliable are finite-size Lyapunov exponents for the assessment of ocean dynamics?. *Ocean Modell* 2011;**36**:208–18. https://doi.org/10.1016/j.ocemod.2010.12.006.

Hernández-Carrasco I, Orfila A, Rossi V *et al.* Effect of small scale transport processes on phytoplankton distribution in coastal seas. *Sci Rep* 2018;**8**:8613–. https://doi.org/10.1038/s41598-018-26857-9.

Hofmann EE, Murphy EJ. Advection, krill, and Antarctic marine ecosystems. *Antarct Sci* 2004;**16**:487–99. https://doi.org/10.1017/S0954102004002275.

Hudson K, Oliver MJ, Bernard K *et al.* Reevaluating the Canyon Hypothesis in a biological hotspot in the Western Antarctic Peninsula. *J Geophys Res Oceans* 2019;**124**:6345–59. https://doi.org/10.1029/2019JC015195.

Huhn F, von Kameke A, Pérez-Muñuzuri V *et al.* The impact of advective transport by the South Indian Ocean Countercurrent on the Madagascar plankton bloom. *Geophys Res Lett* 2012;**39**. https://doi.org/10.1029/2012GL051246.

Kavanaugh MT, Abdala FN, Ducklow H *et al.* Effect of continental shelf canyons on phytoplankton biomass and community composition along the western Antarctic Peninsula. *Mar Ecol Progr Ser* 2015;**524**:11–26. https://doi.org/10.3354/meps11189.

Kohut J. Studying the impacts of local oceanographic processes on Adelie penguin foraging ecology. In: *Marine technology; study data from University of Alaska Update Understanding of Marine Technology*, Vol. **750**. Ecology, environment & conservation (Atlanta). Washington: Marine Technology Society, 2014.

Kohut JT, Roarty HJ, Glenn SM. Characterizing observed environmental variability with HF doppler radar surface current mappers and acoustic doppler current profilers: environmental variability in the coastal ocean. *IEEE J Oceanic Eng* 2006;**31**:876–84. https://doi.org/10.1109/JOE.2006.886095.

Kohut JT, Winsor P, Statscewich H *et al.* Variability in summer surface residence time within a West Antarctic Peninsula biological hotspot. *Philos Trans R Soc Lond Ser A Math Phys Eng Sci* 2018;**376**:20170165.

Lasker R. The relations between oceanographic conditions and larval anchovy food in the California Current: identification of factors contributing to recruitment failure. *Environ Sci* 1978;**173**:212–30.

Lehahn Y, d'Ovidio F, Lévy M *et al.* Stirring of the northeast Atlantic spring bloom: a Lagrangian analysis based on multisatellite data. *J Geophys Res Oceans* 2007;**112**:C08005. https://doi.org/10.1029/2006JC003927.

Lévy M, Franks PJS, Smith KS. The role of submesoscale currents in structuring marine ecosystems. *Nat Commun* 2018;**9**:4758–16. https://doi.org/10.1038/s41467-018-07059-3.

Li W, Tang S, Zhan H. A winter chlorophyll bloom analyzed using Lagrangian diagnoses in the northeastern South China Sea. *Aquat Ecosyst Health Manage* 2015;**18**:462–6.

Liu Y, Wilson C, Green MA *et al.* Gulf stream transport and mixing processes via coherent structure dynamics. *J Geophys Res Oceans* 2018;**123**:3014–37. https://doi.org/10.1002/2017JC013390.

Mahadevan A. The impact of submesoscale physics on primary productivity of plankton. *Ann Rev Mar Sci* 2016;**8**:161–84. https://doi.org/10.1146/annurev-marine-010814-015912.

Martini KI, Stabeno PJ, Ladd C *et al.* Dependence of subsurface chlorophyll on seasonal water masses in the Chukchi Sea. *J Geophys Res Oceans* 2016;**121**:1755–70. https://doi.org/10.1002/2015JC011359.

Mathur M, David MJ, Sharma R *et al.* Thermal fronts and attracting Lagrangian coherent structures in the north Bay of Bengal during December 2015–March 2016. *Deep Sea Res Part II* 2019;**168**:104636. https://doi.org/10.1016/j.dsr2.2019.104636.

Michael ND, Richard KG, Louis WB *et al.* Connectivity in marine protected areas. *Science* 2006;**313**:43–5.

Okubo A. Horizontal dispersion of floatable particles in the vicinity of velocity singularities such as convergences. *Deep Sea Res Oceanogr Abstr* 1970;**17**:445–54. https://doi.org/10.1016/0011-7471(70)90059-8.

Oliver MJ, Irwin A, Moline MA *et al.* Adélie penguin foraging location predicted by tidal regime switching. *PLoS ONE* 2013;**8**:e55163. https://doi.org/10.1371/journal.pone.0055163.

Oliver MJ, Kohut JT, Bernard K *et al.* Central place foragers select ocean surface convergent features despite differing foraging strategies. *Sci Rep* 2019;**9**:157. https://doi.org/10.1038/s41598-018-35901-7.

Paduan JD, Graber HC. Introduction to high-frequency radar: reality and myth. *Oceanography* 1997;**10**:36–9. https://doi.org/10.5670/oceanog.1997.18.

Prants SV, Budyansky MV, Uleysky MY. Identifying Lagrangian fronts with favourable fishery conditions. *Deep Sea Res Part I Oceanogr Res Pap* 2014;**90**:27–35. https://doi.org/10.1016/j.dsr.2014.04.012.

Reister I. isreister/ACROBAT: v1.0.0_UAFOceansACROBAT. v1.0.0UAF_ACROBAT edn. Zenodo, 2023

Saba GK, Fraser WR, Saba VS *et al.* Winter and spring controls on the summer food web of the coastal West Antarctic Peninsula. *Nat Commun* 2014;**5**:4318. https://doi.org/10.1038/ncomms5318.

Schofield O, Ducklow H, Bernard K *et al.* Penguin biogeography along the West Antarctic Peninsula: testing the Canyon Hypothesis with Palmer LTER observations. *Oceanography* 2013;**26**:204–6. https://doi.org/10.5670/oceanog.2013.63.

Serra M, Sathe P, Rypina I *et al.* Search and rescue at sea aided by hidden flow structures. *Nat Commun* 2020;**11**:2525. https://doi.org/10.1038/s41467-020-16281-x.

Shadden SC, Lekien F, Marsden JE. Definition and properties of Lagrangian coherent structures from finite-time Lyapunov exponents in two-dimensional aperiodic flows. *Phys D* 2005;**212**:271–304. https://doi.org/10.1016/j.physd.2005.10.007.

Shadden SC, Lekien F, Paduan JD *et al.* The correlation between surface drifters and coherent structures based on high-frequency radar data in Monterey Bay. *Deep Sea Res Part II Top Stud Oceanogr* 2009;**56**:161–72. https://doi.org/10.1016/j.dsr2.2008.08.008.

Siegelman L, Klein P, Rivière P *et al.* Enhanced upward heat transport at deep submesoscale ocean fronts. *Nat Geosci* 2020;**13**:50–5. https://doi.org/10.1038/s41561-019-0489-1.

St-Onge-Drouin S, Winkler G, Dumais J-F *et al.* Hydrodynamics and spatial separation between two clades of a copepod species complex. *J Mar Syst* 2014;**129**:334–42. https://doi.org/10.1016/j.jmarsys.2013.07.014.

Statscewich H, Weingartner T. *A High-Latitude Modular Autonomous Power, Control, and Communication System for Application to High-Frequency Surface Current Mapping Radars*. New York: IEEE. 2011, 1–3.

Stewart RH, Joy JW. HF radio measurements of surface currents. *Deep Sea Res Oceanogr Abstr* 1974;**21**:1039–49. https://doi.org/10.1016/0011-7471(74)90066-7.

Tew Kai E, Rossi V, Sudre J *et al.* Top marine predators track Lagrangian coherent structures. *Proc Natl Acad Sci* 2009;**106**:8245–50. https://doi.org/10.1073/pnas.0811034106.

Thomalla SJ, Racault M-F, Swart S *et al.* High-resolution view of the spring bloom initiation and net community production in the Subantarctic Southern Ocean using glider data. *ICES J Mar Sci* 2015;**72**:1999–2020. https://doi.org/10.1093/icesjms/fsv105.

Veatch J, Fredj E, Kohut J. High frequency radars as ecological sensors: using Lagrangian coherent structures to quantify prey concentrating features. In: *OCEANS 2022, Hampton Roads*. New York: IEEE, 2022, **2022**, 1–7.

Watson JR, Fuller EC, Castruccio FS *et al.* Fishermen follow fine-scale physical ocean features for finance. *Frontiers in Marine Science* 2018;**5**. https://doi.org/10.3389/fmars.2018.00046.

Weiss J. The dynamics of enstrophy transfer in two-dimensional hydrodynamics. *Phys D* 1991;**48**:273–94. https://doi.org/10.1016/0167-2789(91)90088-Q.

Handling Editor: Rubao Ji